Controllable spontaneous resolution in ultrasmall Cu-Ag bimetallic cluster ion pairs from achiral components

Jiao He, Cheng-Long Deng, Cun-Fa Sun, Xiao-Xiao Zhang, Ying Cui, Sheng-Hui Wu,* and Geng-Geng Luo*

Electronic Supplementary Information (ESI)

Fig. S1-S21 & Table S1-S4

Physical measurements

^{1}H NMR and ^{31}P NMR spectra at room temperature were recorded on a Bruker Avance III 500 MHz NMR spectrometer and chemical shifts (in ppm) were referred to $CDCl_3$ (δ = 7.26 ppm), as an internal standard. Mass spectra were recorded on an Agilent 6224 (Agilent Technologies, USA) ESI-TOF-MS spectrometer. Sample solutions are infused by a syringe pump at 4 μL/min. Data were acquired using the following settings: ESI capillary voltage was set at 3500 V (−) ion mode and fragmentor at 200 V. The liquid nebulizer was set to 15 psig and the nitrogen drying gas was set to a flow rate of 4 L/min. Drying gas temperature was maintained at 150 ^{o}C. The data analyses of mass spectra were performed based on the isotope distribution patterns using Agilent Mass Hunter Workstation Data acquisition software (Version B.05.00). The reported *m/z* values represent monoisotopic mass of the most abundant peak within the isotope pattern. UV-vis absorption spectra were recorded on a PerkinElmer Lambda 1050 UV-vis spectrophotometer. Energy-dispersive X-ray spectrum was measured using an Apreo S LoVac field emission scanning electron microscope (FESEM; ThermoFisher Ltd., America) equipped with a Bruker XFlash energy-dispersive X-ray (EDX; Bruker, German).

Chemical reagents

$Cu(CF_3CO_2)_2 \cdot H_2O$, $AgNO_3$, Cyclohexanethiol (CySH), *tert*-butylthiol (^{t}BuSH), Tetraphenyl phosphonium chloride (PPh_4Cl), Methyl(triphenyl)phosphonium chloride (PPh_3MeCl), (Ethyl)triphenylphosphonium chloride (PPh_3EtCl), (1-Propyl)triphenylphosphonium chloride (PPh_3PrCl) were purchased from Energy Chemical Reagent Co. Ltd. (Shanghai, China). Sodium borohydride ($NaBH_4$), triethylamine (Et_3N), dichloromethane (CH_2Cl_2), methanol (MeOH) and *n*-hexane were purchased from Sinopharm Chemical Reagent Co. Ltd. (Shanghai, China). All chemicals and solvents for synthesis were used without further purification.

Syntheses

The precursors $(CySAg)_n$ and $(^{t}BuSAg)_n$ were prepared according to the

literature[S1].

Synthesis of $(PPh_4)[Cu_2Ag_3(SCy)_6]$ (1): 29.1 mg $Cu(CF_3CO_2)_2 \cdot H_2O$ was dissolved in 1 mL methanol solution, and added to 1 mL methanol solution containing 23.2 mg $(CySAg)_n$, resulting in a thick light green mixture. After stirring for 5 min, 37.5 mg PPh_4Cl in 2 mL CH_2Cl_2 was added to the reaction solution for 10 min. 66 μL CySH was added, the reaction solution turned pale yellow. After 40 min, 1 mL ice-cold aqueous solution of 40 mg $NaBH_4$ with 50 μL Et_3N was added dropwise under vigorous stirring. Then, the color of the solution changed immediately from pale yellow to deep reddish brown. After aging at room temperature for 8 h, the organic phase was washed with distilled water several times to remove the organic phase, dissolved in dichloromethane and centrifuged at 8000 r/min for 3 min. By diffusing *n*-hexane to reddish brown solutions of dichloromethane and kept for single crystal growth at -18 ^oC in a freezer.

Synthesis of $(PPh_3Me)[(Cu_2Ag_3(SCy)_6]$ (2): The synthesis procedure of **2** was identical to that of **1** except that PPh_3MeCl was used instead of PPh_4Cl.

Synthesis of $(PPh_3Et)[(Cu_2Ag_3(SCy)_6]$ (3): The synthesis procedure of **3** was identical to that of **2** except that PPh_3EtCl was used instead of PPh_3MeCl.

Synthesis of $(PPh_3Pr)[(Cu_2Ag_3(SCy)_6]$ (4): The synthesis procedure of **4** was identical to that of **2** except that PPh_3PrCl was used instead of PPh_3MeCl.

Synthesis of $(PPh_4)[(Cu_2Ag_3(SBu^t)_6]$ (5): The synthesis procedure of **5** was identical to that of **1** except that $(^tBuSAg)_n$ and ^tBuSH used instead of $(CySAg)_n$ and CySH.

Single-crystal X-ray structure determination

Single crystals of **1-5** with appropriate dimensions was chosen under an optical microscope and quickly coated with high vacuum grease (Dow Corning Corporation). Intensity diffraction data of was collected at 173 K on a Rigaku Oxford Diffraction XtaLAB system Synergy diffractometer equipped with a HyPix-6000HE area detector, using a Cu Kα radiation (λ = 1.54184 Å) from PhotonJet micro-focus X-ray source. The

diffraction images were processed and scaled using the CrysAlisPro software. [S2] The structures were solved using the charge-flipping algorithm, as implemented in the program SUPERFLIP[S3] and refined by full-matrix least-squares techniques against F_o^2 using the SHELXL program[S4] through the OLEX2 interface.[S5] Hydrogen atoms at carbon were placed in calculated positions and refined isotropically by using a riding model. Appropriate restraints or constraints were applied to the geometry and atomic displacement parameters of the atoms in the cluster. All structures were examined using the Addsym subroutine of PLATON[S6] to ensure that no additional symmetry could be applied to the models. CCDC Nos for *C*-**1**: CCDC 2076947; *A*-**1**: 2076948; **2**: 2076939; **3**: 2076933; **4**: 2076940; **5**: 2076941.

Computational methods

Full geometry optimizations of [(*C*)-$Cu_2Ag_3(SMe)_6$]$^-$ and [(*A*)-$Cu_2Ag_3(SMe)_6$]$^-$ were performed by density functional theory (DFT) calculations using the ORCA 4.0 version program package[S7] with the BP86 functional[S8] and the all-electron Def2-SVP set from EMSL Basis Set Exchange Library.[S9]

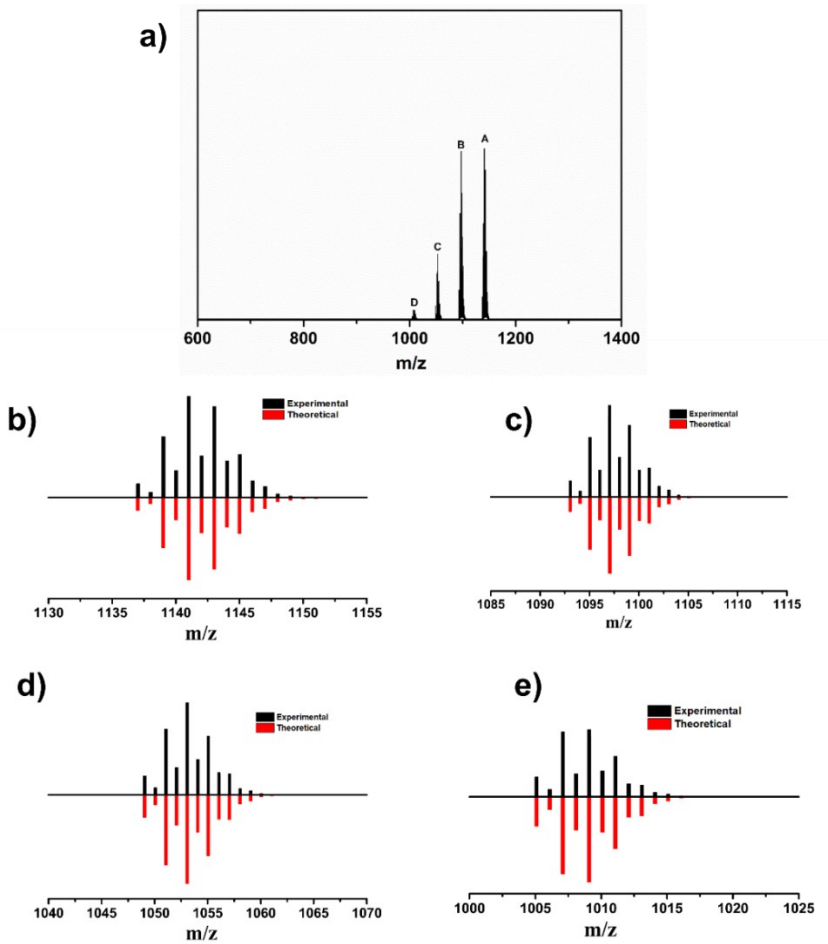

Fig. S1 a) The ESI-MS spectra for **1** in the positive mode (the peaks A-D indicate the metal exchanging occurs in the $[Cu_2Ag_3(SCy)_6]^-$). b) The experimental and theoretical isotopic patterns of molecular ion peak A $[Cu_2Ag_3(SCy)_6]^-$; c) peak B $[Cu_3Ag_2(SCy)_6]^-$; d) peak C $[Cu_4Ag_1(SCy)_6]^-$; and e) peak D $[Cu_5(SCy)_6]^-$.

Comment: The negative-ion ESI-MS of **1** showed four peaks centered at *m*/*z* = 1441.024, 1097.041, 1053.059, 1009.098 (**Fig. S1**). The careful analysis on the high-resolution mass data revealed that the peak at *m*/*z* = 1441.024 corresponds to the molecular ion of $[Cu_2Ag_3(SCy)_6]^-$ (calcd. 1440.923) whose isotopic pattern perfectly matched the simulation. The other three peaks could be assigned to the metal-exchanging species $[Cu_3Ag_2(SCy)_6]^-$, $[Cu_4Ag(SCy)_6]^-$, and $[Cu_5(SCy)_6]^-$, respectively. Notably, the phenomenon of coinage-metal exchange in the alloy clusters has been described before.[S10]

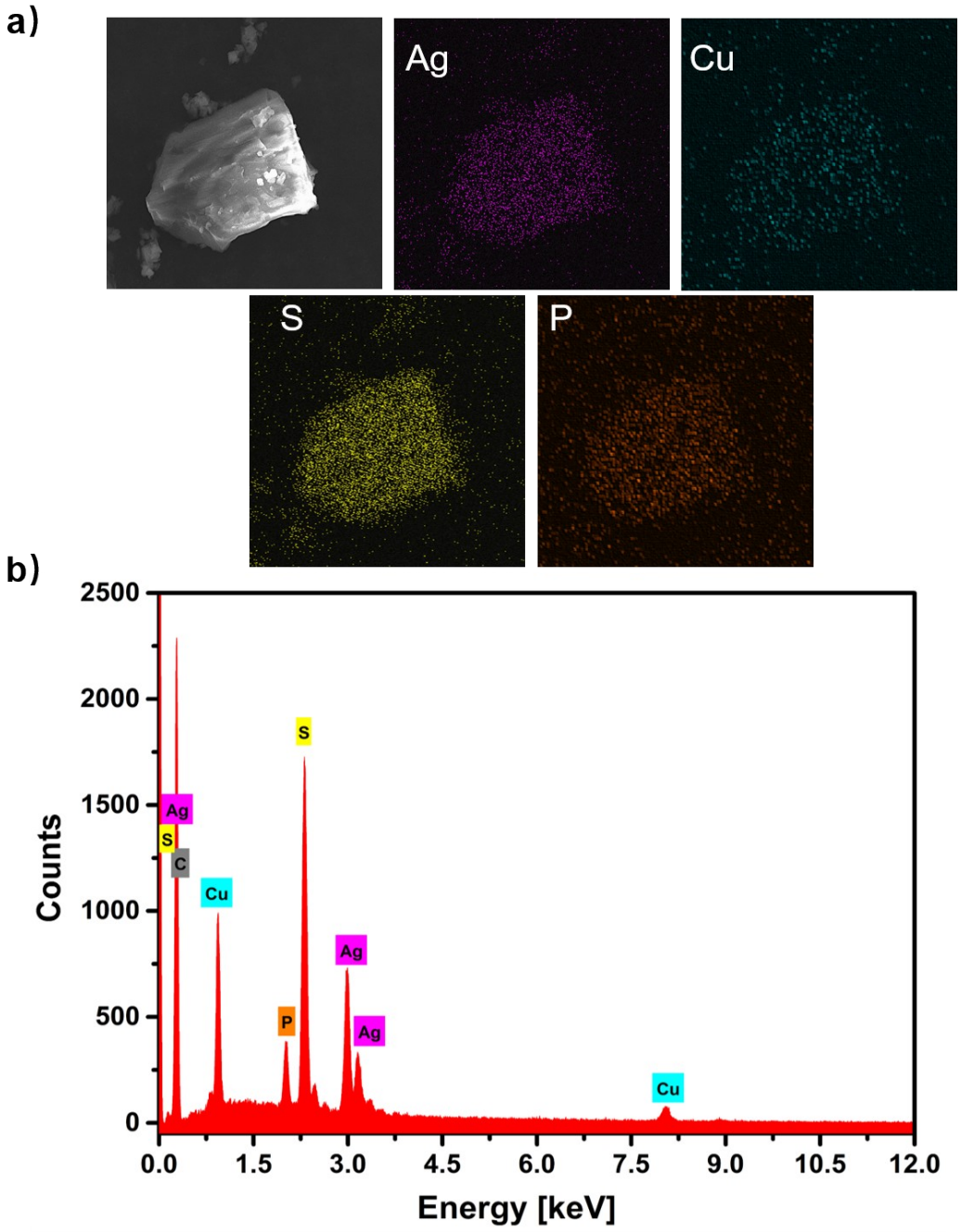

Fig. S2 a) SEM imaging of **1** used for mapping analyses. b) EDX spectrum of **1**.

Comment: The metal composition of **1** was also probed by energy dispersive X-ray spectra (EDX) data (**Fig. S2**), showing the Cu/Ag atomic ratio to be 2.3:2.7.

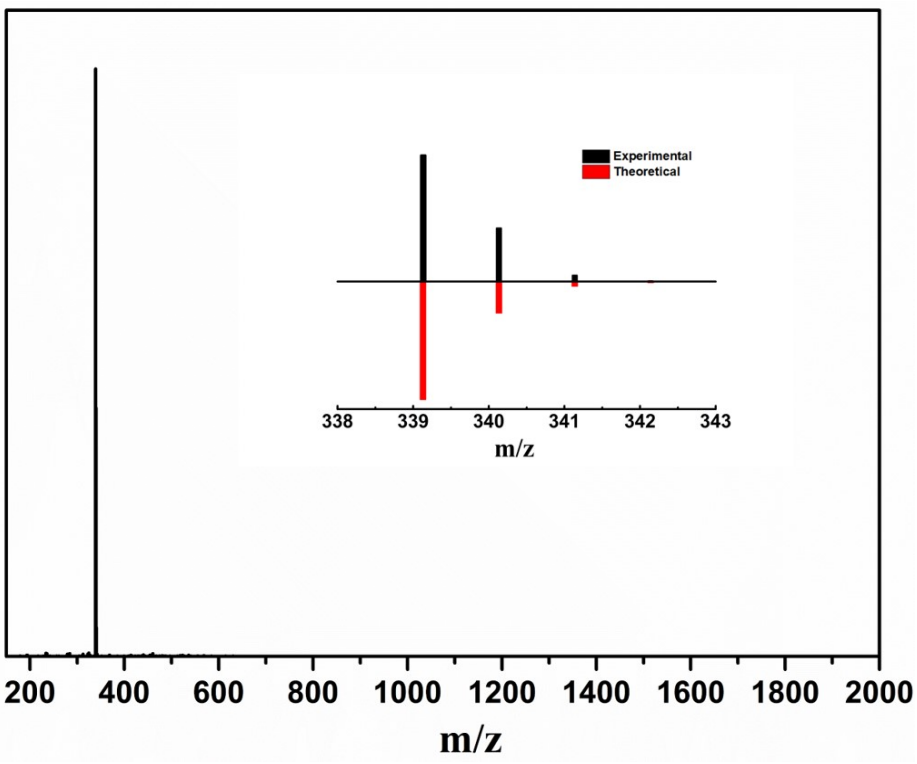

Fig. S3 Measured and simulated positive-ion ESI-MS spectrum of **1** in CH_2Cl_2.

Comment: We see a dominant peak in the positive-ion mode corresponding to the counter-cation PPh_4^+ (**Fig. S3**).

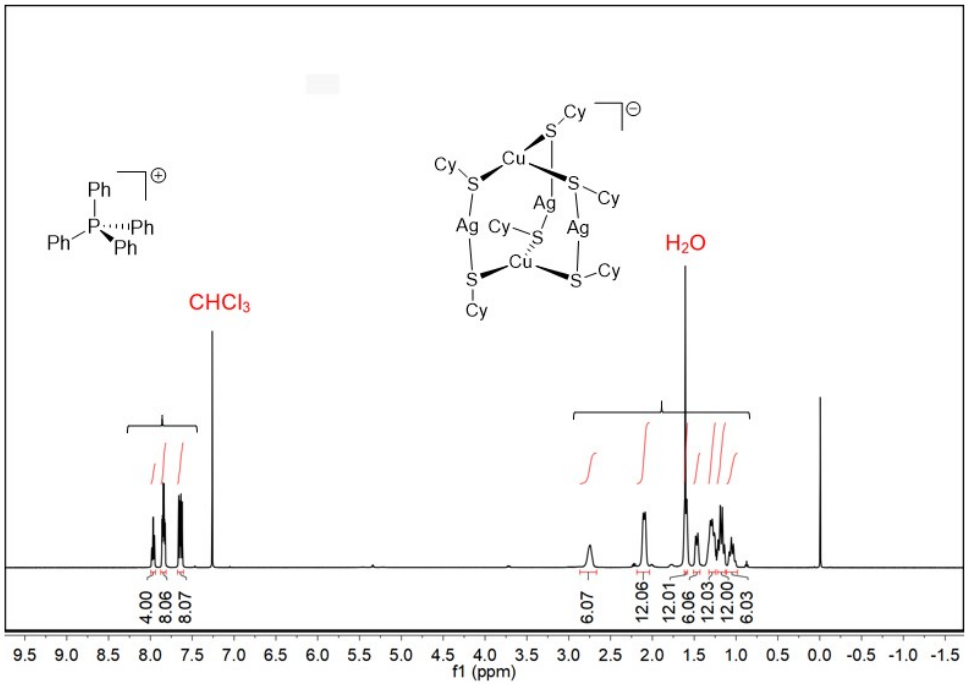

Fig. S4 ^{1}H NMR spectrum of **1** in $CDCl_3$ at room temperature. ^{1}H NMR (500 MHz, $CDCl_3$): δ = 7.95-7.99 ppm (m, 4H, PPh_4), δ =7.82-7.86 ppm (m, 8H, PPh_4), δ =7.62-7.66 ppm (m, 8H, PPh_4), δ = 2.72-2.81 ppm (m, 6H, CyS), δ = 2.08-2.11 ppm (m, 12H, CyS), δ = 1.62-1.58 ppm (m, 12H, CyS), δ = 1.45-1.49 ppm (m, 6H, CyS), δ = 1.25-1.32 ppm (m, 12H, CyS), δ = 1.13-1.23 ppm (m, 12H, CyS), δ = 1.01-1.08 ppm (m, 6H, CyS), δ = 7.26 ppm ($CDCl_3$), δ = 1.61 ppm (H_2O).

Comment: The ^{1}H NMR spectrum of **1** recorded in $CDCl_3$ is diamagnetic, precluding the presence of Cu^{2+}, and displays clearly resolved signals, all of which can be unambiguously assigned (**Fig. S4**).

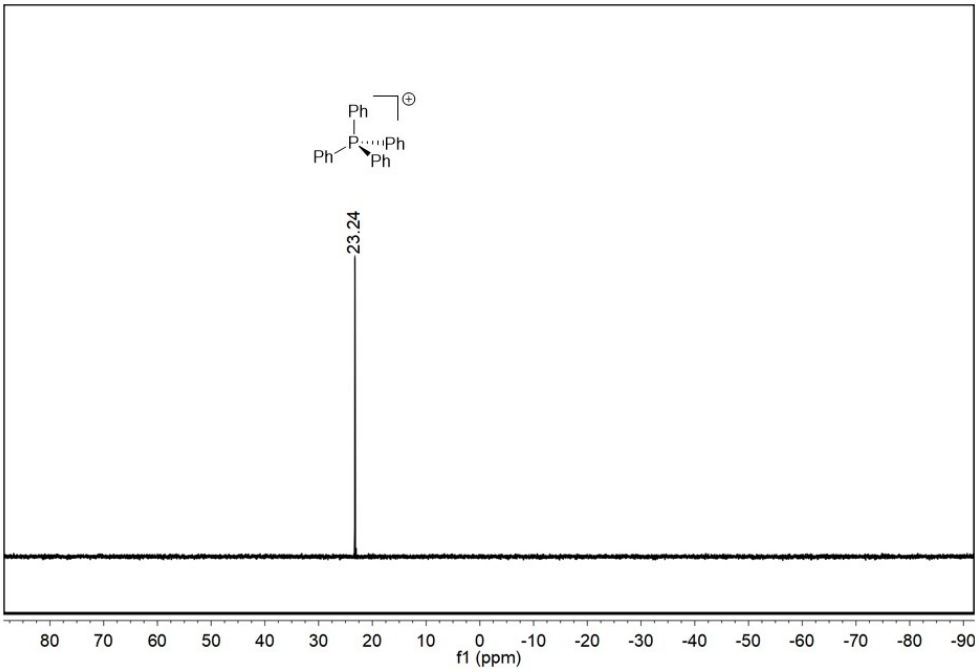

Fig. S5 ^{31}P NMR spectrum of **1** in $CDCl_3$. ^{31}P NMR (200 MHz, $CDCl_3$): δ = 23.34 ppm (s, PPh_4).

Comment: ^{31}P NMR spectrum of **1** (**Fig. S5**) shows a single peak at δ = 23.24 ppm corresponding to PPh_4^+ species.

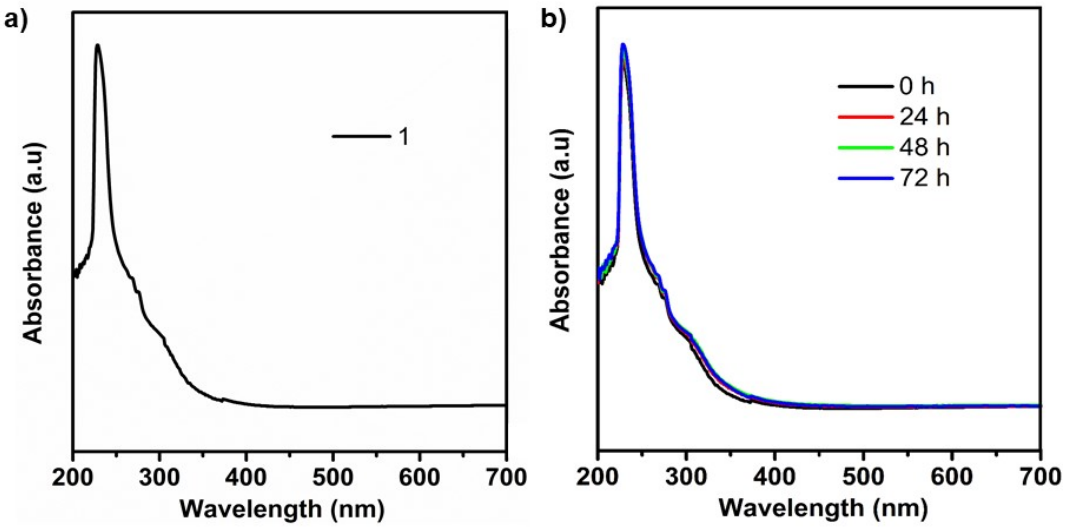

Fig. S6 a) UV-vis absorbance spectra of **1** in the CH_2Cl_2. b) The time-dependent UV-vis absorbance spectra of **1** (10^{-5} M) in the CH_2Cl_2 under ambient conditions.

Comment: The UV-vis absorption spectrum of **1** in CH_2Cl_2 exhibits a combination of absorption features from their specific subunits of cationic PPh_4^+ and anionic $[Cu_2Ag_3(SCy)_6]^-$ (**Fig. S6a**). **1** possesses good stability in solution, as evidenced by time-dependent absorption spectra showing no obvious change within 72 h (**Fig. S6b**).

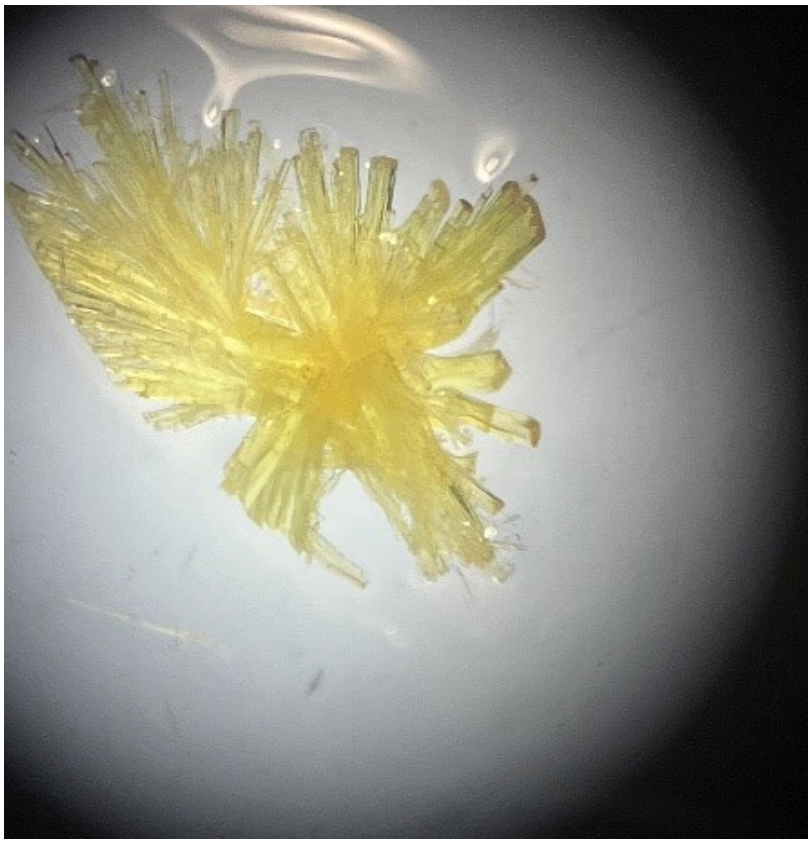

Fig. S7 Single crystals of *C*-**1** and *A*-**1** under the microscope

(**a**)

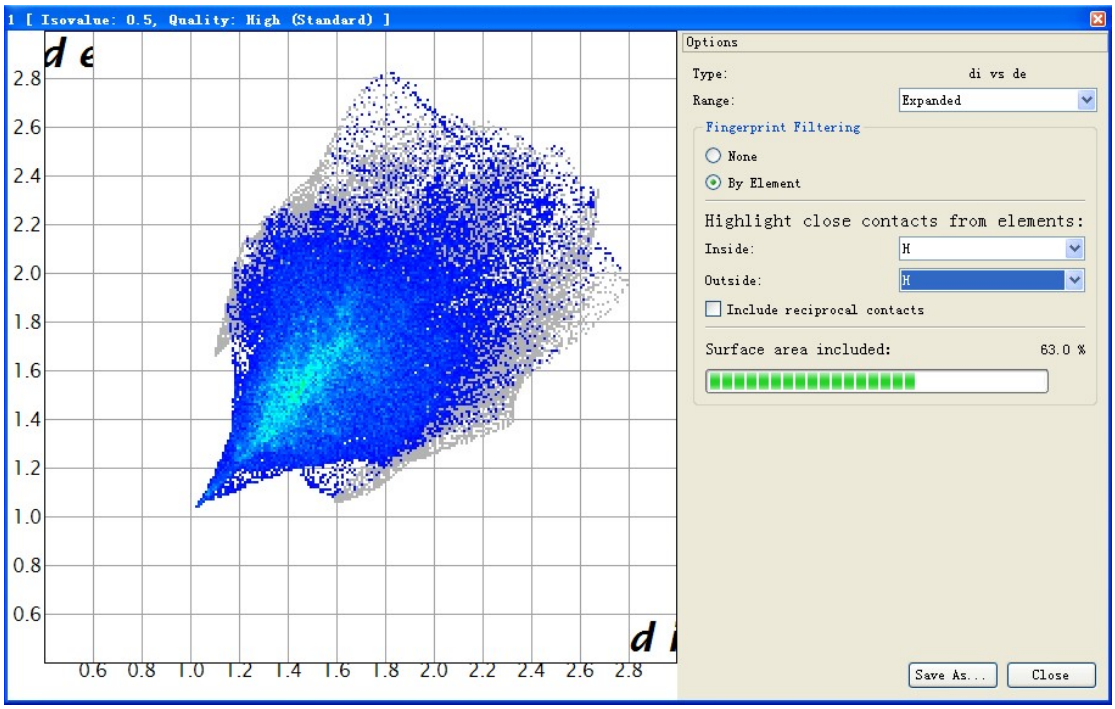

(**b**)

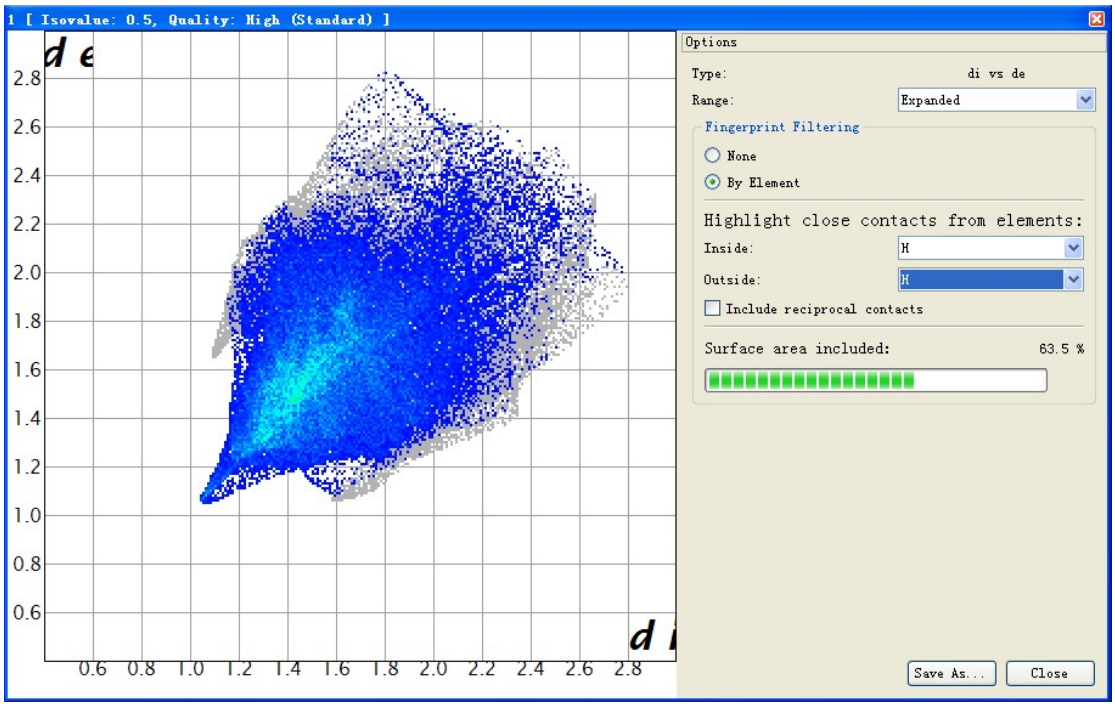

Fig. S8 2D fingerprint plot analyses (including important H···H contacts) of *C*-**1** (a) and *A*-**1** (b).

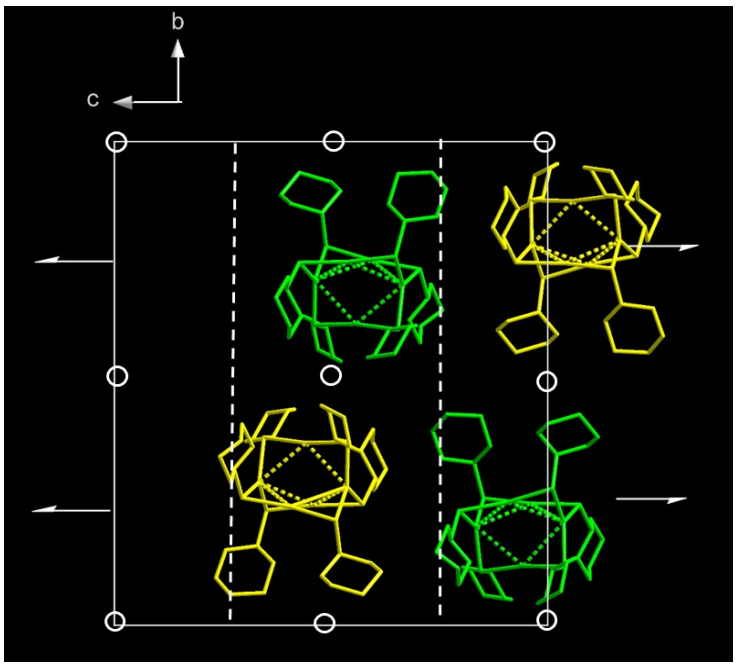

Fig. S9 The heterochiral packings in the racemic crystals **3** viewed down *a*. Different colors distinguish the two enantiomers ([(*A*)-$Cu_2Ag_3(SCy)_6$]$^-$ and [(*C*)-$Cu_2Ag_3(SCy)_6$]$^-$. All the H atoms, cations and solvents have been omitted for clarity.

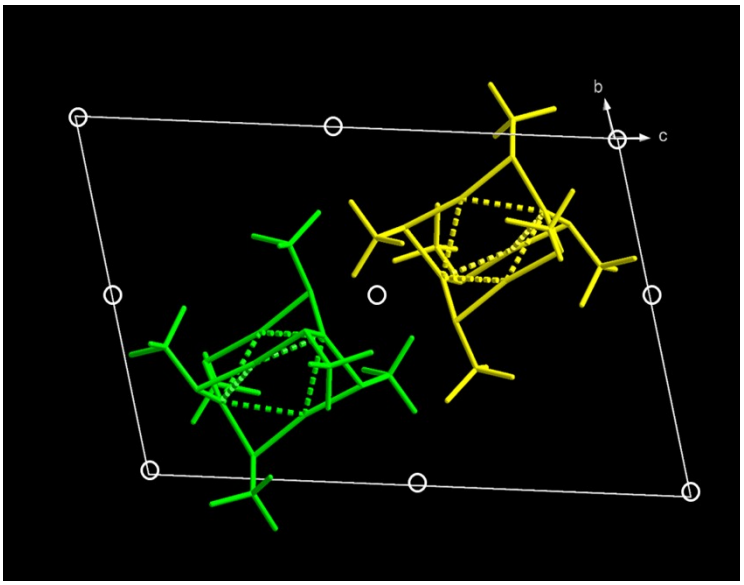

Fig. S10 The heterochiral packings in the racemic crystals **5** viewed down *a*. Different colors distinguish the two enantiomers ([(*A*)-$Cu_2Ag_3(SBu^t)_6$]$^-$ and ([(*C*)-$Cu_2Ag_3(SBu^t)_6$]$^-$). All the H atoms, cations and solvents have been omitted for

clarity.

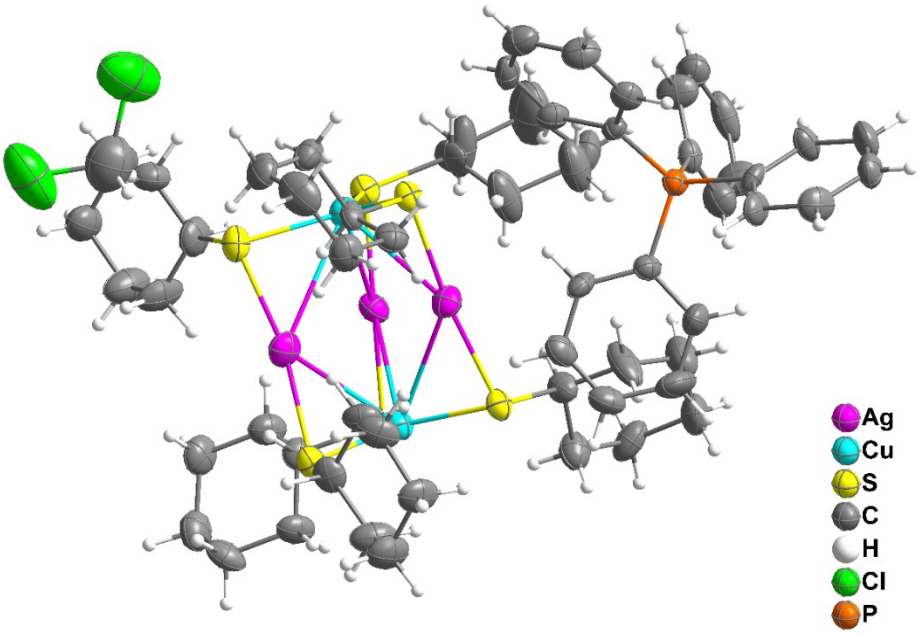

Fig. S11 The thermal ellipsoids of the ORTEP diagram of *C*-**1**.

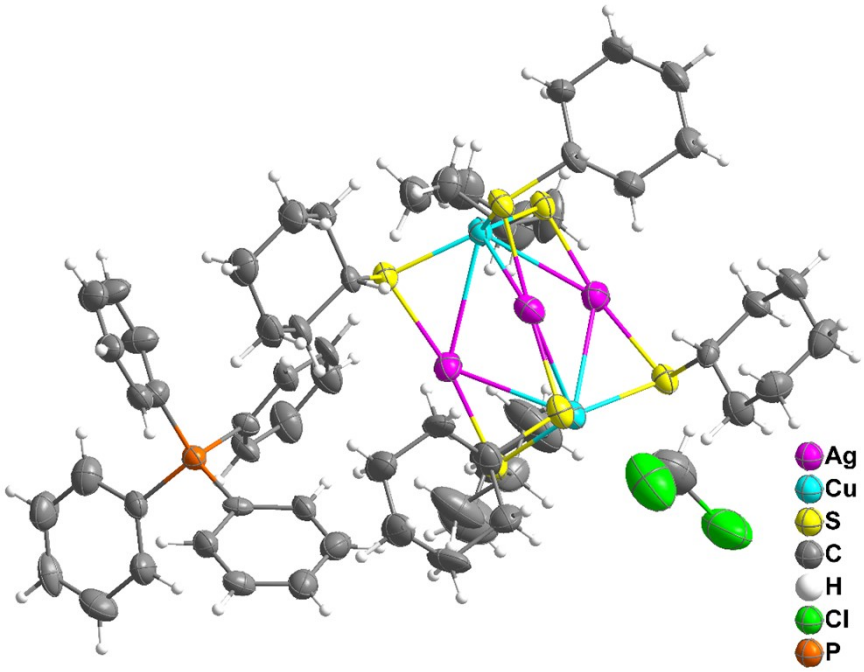

Fig. S12 The thermal ellipsoids of the ORTEP diagram of *A*-**1**.

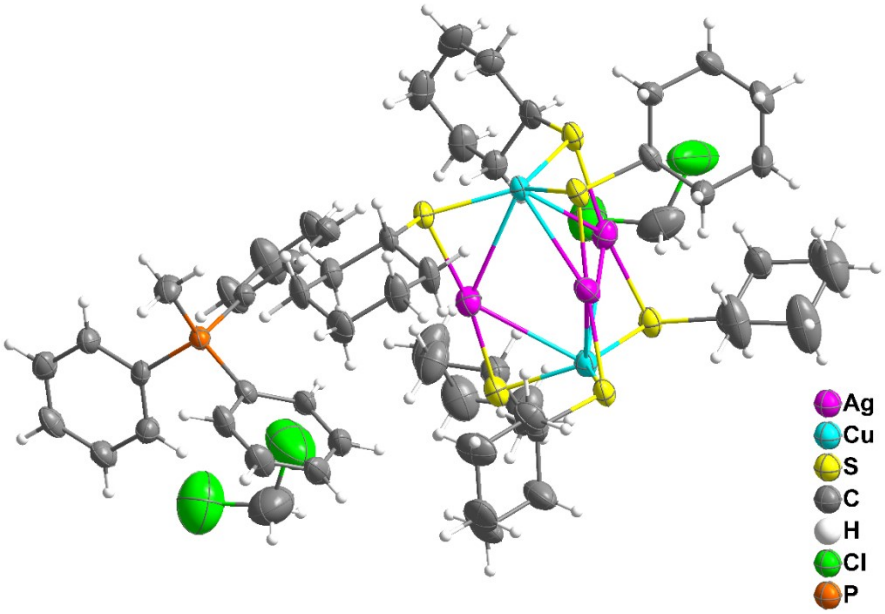

Fig. S13 The thermal ellipsoids of the ORTEP diagram of **2**.

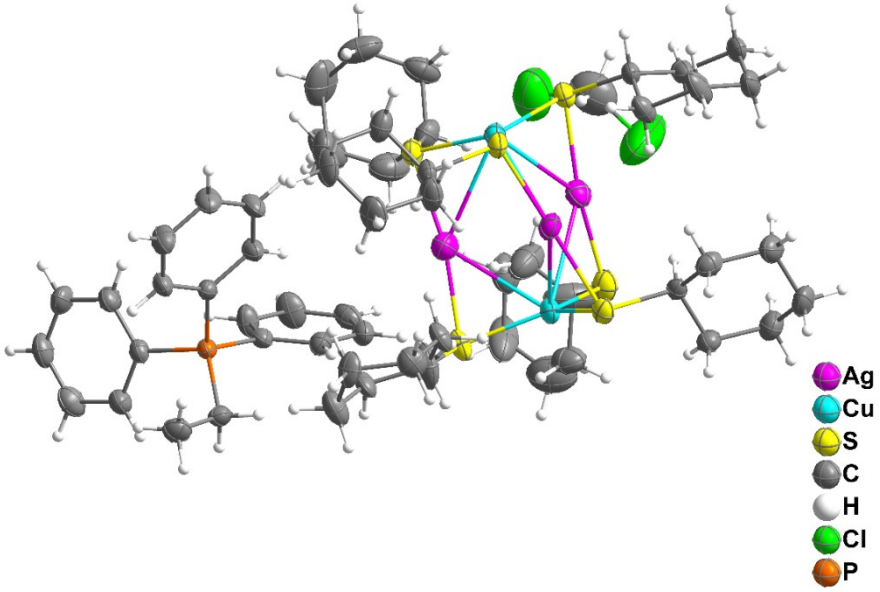

Fig. S14 The thermal ellipsoids of the ORTEP diagram of **3**.

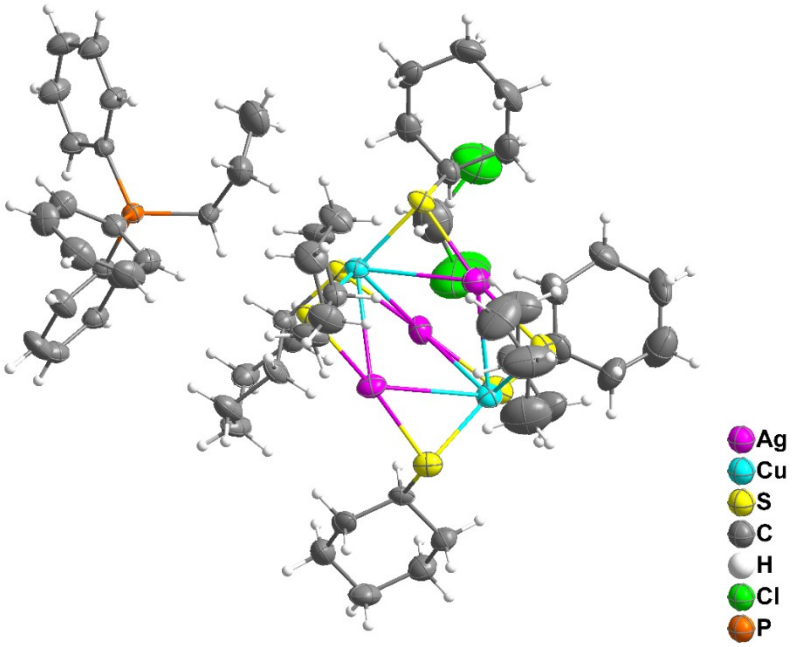

Fig. S15 The thermal ellipsoids of the ORTEP diagram of **4**.

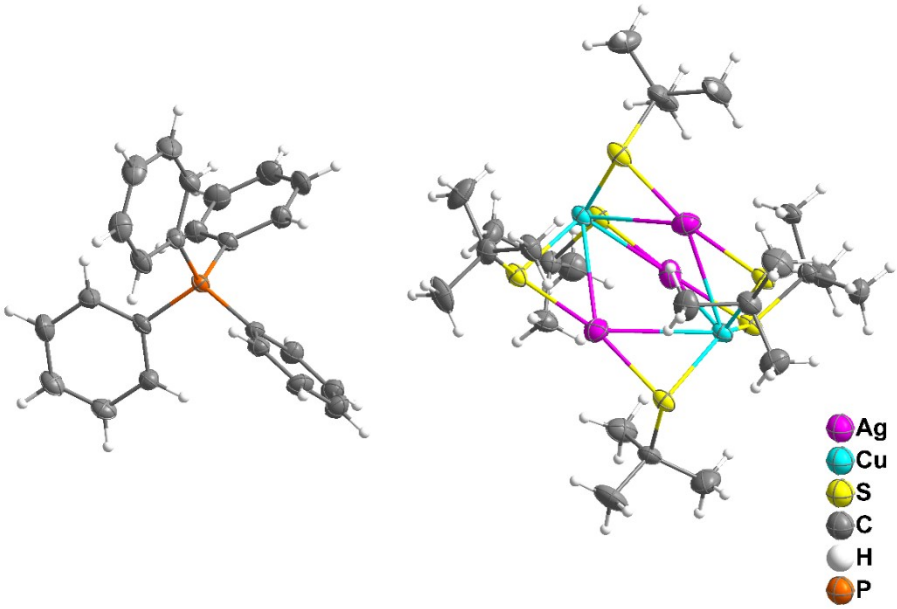

Fig. S16 The thermal ellipsoids of the ORTEP diagram of **5**.

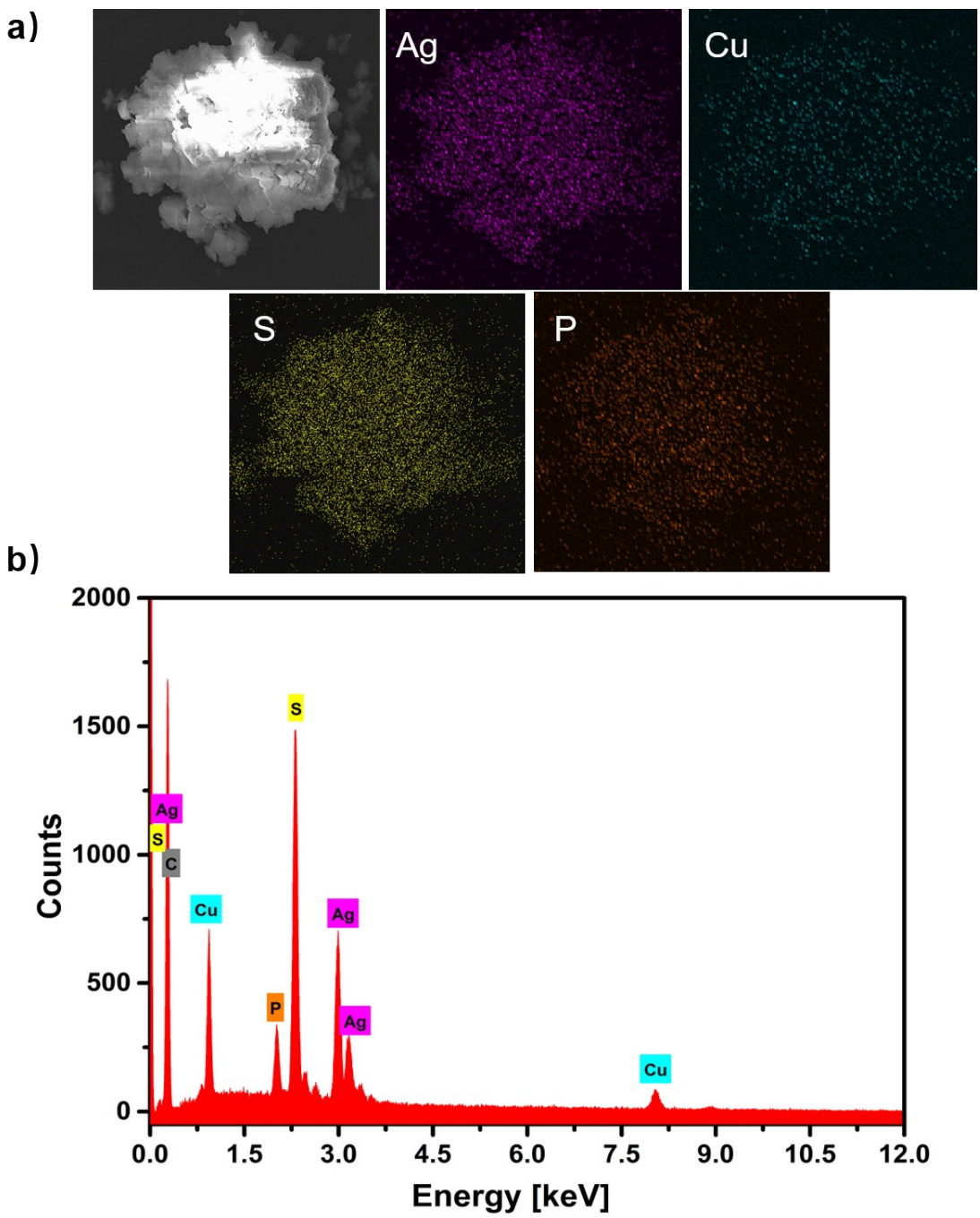

Fig. S17 a) SEM imaging of **2** used for mapping analyses. b) EDX spectrum of **2**.

Comment: The metal composition of **2** was probed by SEM mapping and energy dispersive X-ray spectra (EDX) data (**Fig. S17**). The EDX result gave the Cu/Ag atomic ratio to be 2.4:2.6.

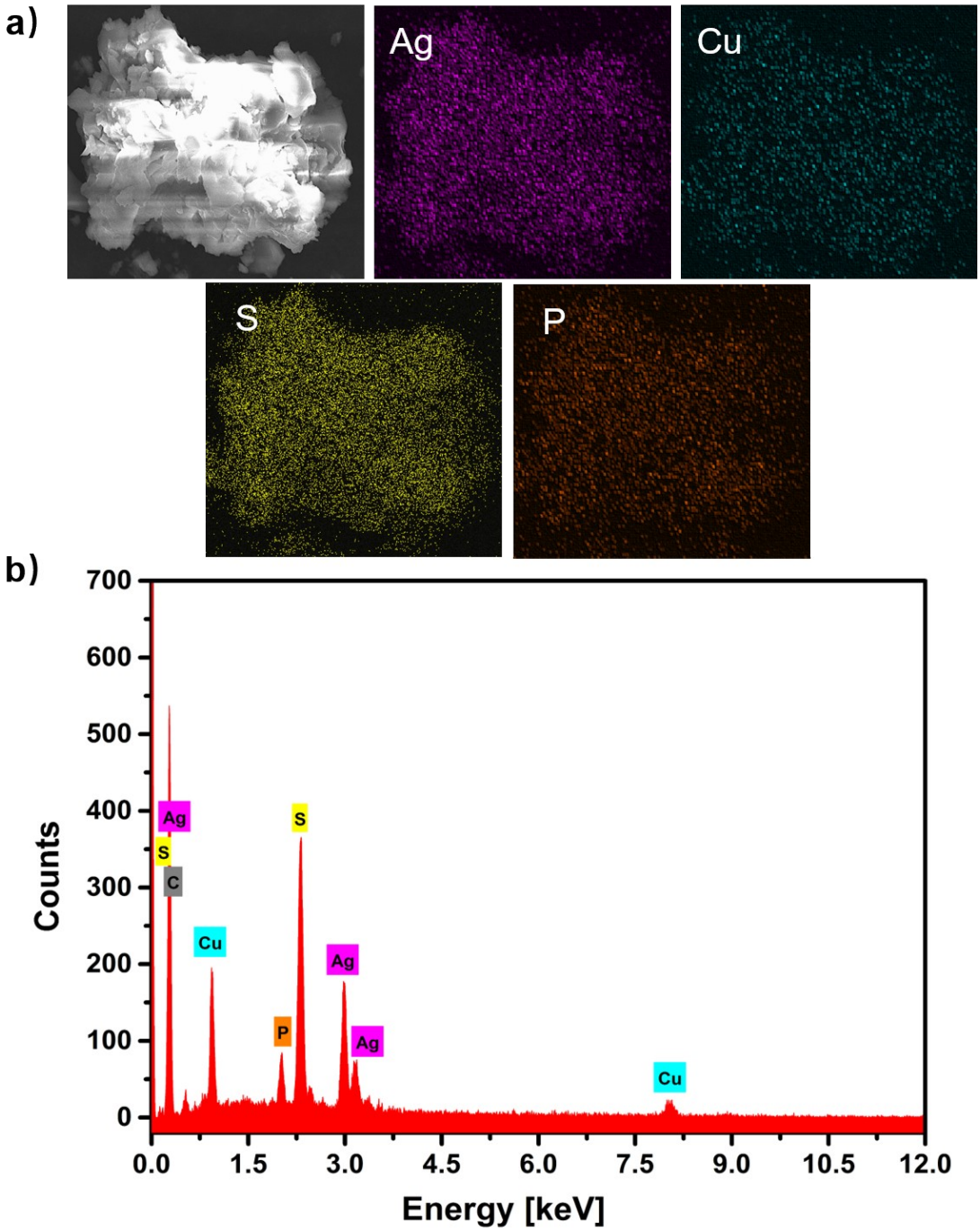

Fig. S18 a) SEM imaging of **3** used for mapping analyses. b) EDX spectrum of **3**.

Comment: The metal composition of **3** was probed by SEM mapping and energy dispersive X-ray spectra (EDX) data (**Fig. S18**). The EDX result gave the Cu/Ag atomic ratio 2.2:2.8.

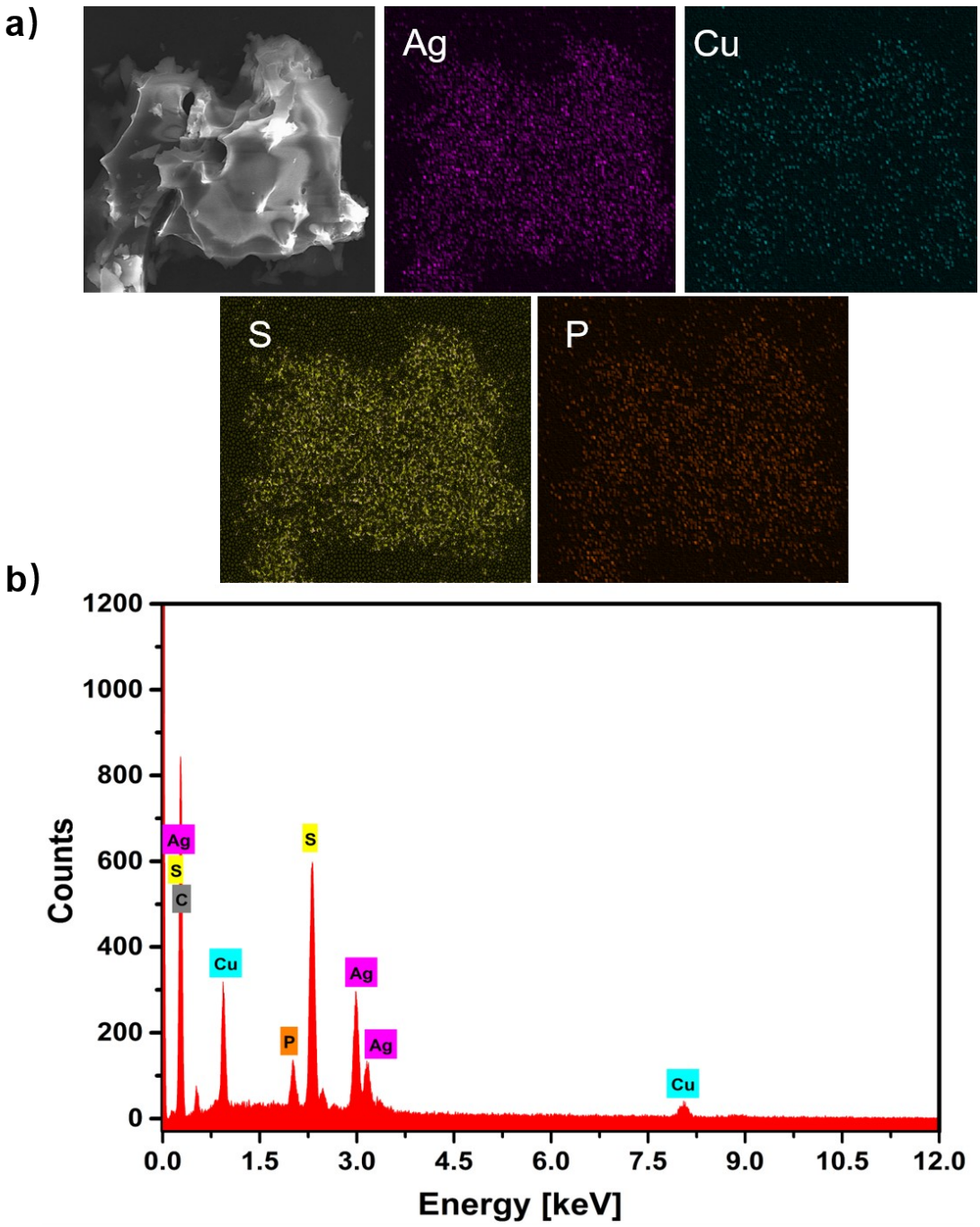

Fig. S19 a) SEM imaging of **4** used for mapping analyses. b) EDX spectrum of **4**.

Comment: The metal composition of **4** was probed by SEM mapping and energy dispersive X-ray spectra (EDX) data (**Fig. S19**). The EDX result gave the Cu/Ag atomic ratio to be 2.2:2.8 for **4**.

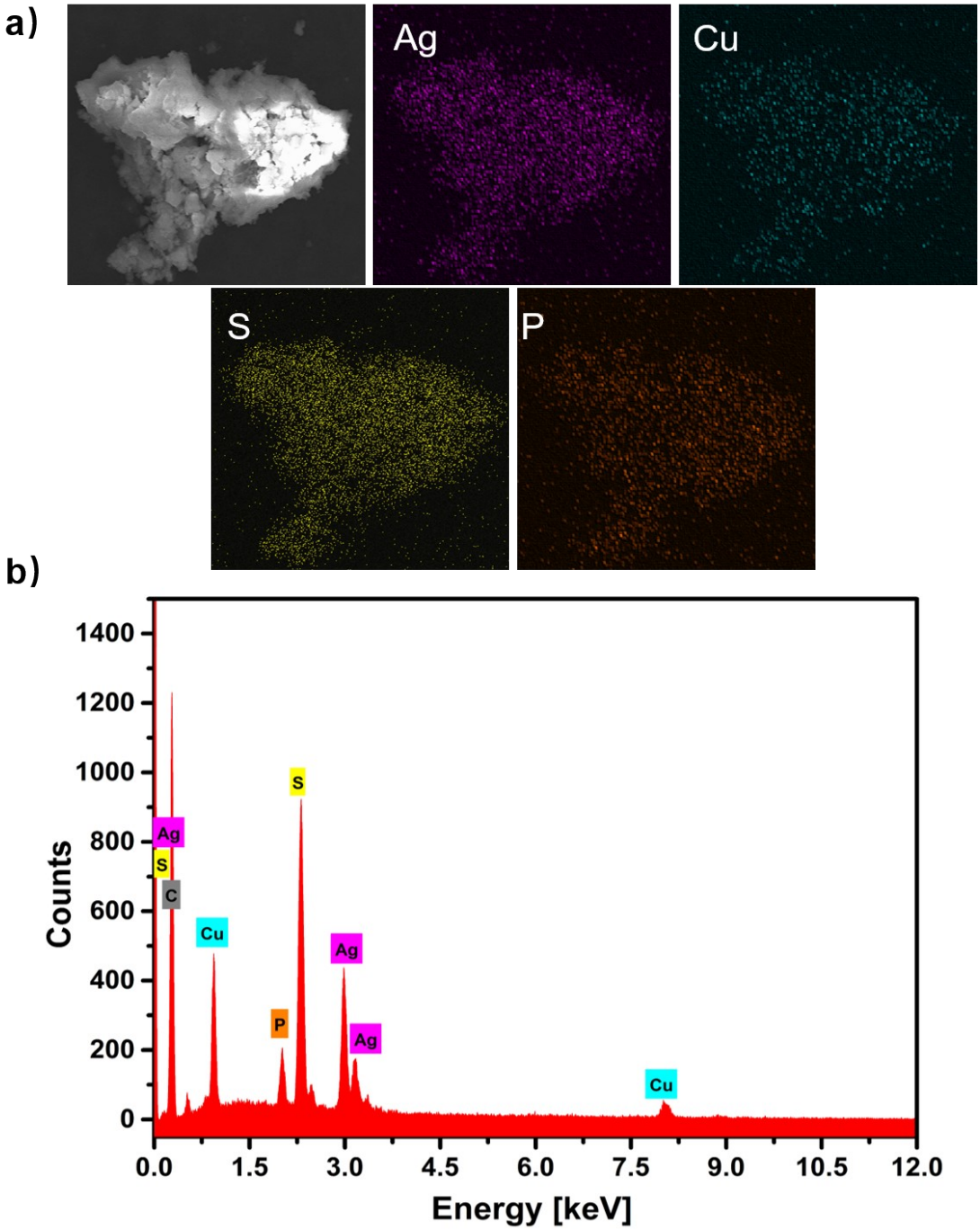

Fig. S20 a) SEM imaging of **5** used for mapping analyses. b) EDX spectrum of **5**.

Comment: The metal composition of **5** was probed by SEM mapping and energy dispersive X-ray spectra (EDX) data (**Fig. S20**). The EDX result gave the Cu/Ag atomic ratio to be 2.3:2.7.

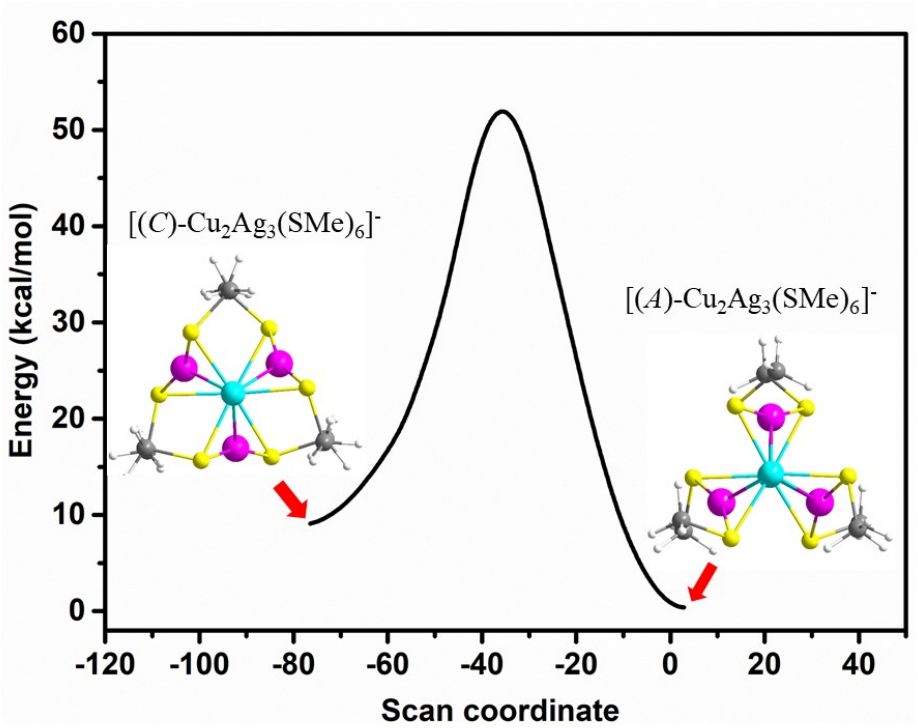

Fig. S21 Energy profile of the transition state of enantiomeric cluster ([(*C*)-$Cu_2Ag_3(SMe)_6]^-$ and [(*A*)-$Cu_2Ag_3(SMe)_6]^-$).

Comment: Let us note that in the reported thiolate-protected gold nanocluster $Au_{38}(SCH_2CH_2Ph)_{24}$, the chiral inversion of two gold cluster-based enantiomers proceeds via core reconstruction without breaking a Au-S bond due to the low activation barrier (28.1 kcal mol^{-1}).[S11] By comparison, theoretical calculations using the methylthiolate (SCH_3) to model the thiolate ligands in **1** indicate that the activation barrier for the racemization of $[Cu_2Ag_3(SMe)_6]^-$, as high as up to 55.6 kcal mol^{-1} (**Fig. S21**). The energy profile of the transition state is high enough to lock each enantiomeric cluster ([(*C*)-$Cu_2Ag_3(SCH_3)_6]^-$ **and** [(*A*)-$Cu_2Ag_3(SCH_3)_6]^-$) into its geometry, which implies that the chemically improbable dissociation of all six thiolate ligands and interconversion of the enantiomer clusters is excluded.

Table S1 Crystallographic data and structure refinements results for ***C*-1** and ***A*-1**

Cluster complex	***C*-1**	***A*-1**
Empirical formula	$C_{61}H_{88}Ag_3Cl_2Cu_2PS_6$	$C_{61}H_{88}Ag_3Cl_2Cu_2PS_6$
Formula weight	1566.23	1566.23
Temperature/K	190.00(10)	190.00(10)
Crystal system	orthorhombic	orthorhombic
Space group	$P2_12_12_1$	$P2_12_12_1$
a/Å	13.7428(5)	13.7242(3)
b/Å	20.2094(8)	20.2084(6)
c/Å	26.5743(13)	26.4773(9)
α/°	90	90
β/°	90	90
γ/°	90	90
Volume/Å^3	7380.6(5)	7343.3(4)
Z	4	4
ρ_{calc}g/cm^3	1.410	1.417
μ/mm^{-1}	1.645	1.653
F(000)	3192.0	3192.0
Crystal size/mm^3	0.33 × 0.25 × 0.2	0.33 × 0.25 × 0.2
Radiation	Mo Kα (λ = 0.71073)	Mo Kα (λ = 0.71073)
2θ range for data collection/°	4.264° to 58.784°	3.904 ° to 58.826 °
Index ranges	-15 ≤ h ≤ 17, -25 ≤ k ≤ 27, -35 ≤ l ≤ 20	-11 ≤ h ≤ 18, -17 ≤ k ≤ 26, -28 ≤ l ≤36
Reflections collected	29526	28701
Independent reflections	16072 [R_{int} = 0.0387, R_{sigma} = 0.0809]	16024[R_{int} =0.0393, R_{sigma} = 0.0793]
Data/restraints/parameters	16072/42/676	16024/42/676
Goodness-of-fit on F^2	1.012	0.993
Final R indexes [I>=2σ (I)]	R_1 = 0.0586, wR_2 = 0.1156	R_1 = 0.0532, wR_2 = 0.1200
Final R indexes [all data]	R_1 = 0.0779, wR_2 = 0.1254	R_1 =0.0803, wR_2 = 0.1361
Flack parameter	-0.024(11)	-0.009(11)

Table S2 Selected bond lengths for *C*-**1** and *A*-**1.**

***C*-1**			
Atom-Atom	Bond length/ Å	Atom-Atom	Bond length/ Å
Ag1-Cu1	2.9015(13)	Ag3-Cu2	2.9909(12)
Ag3-S3	2.365(2)	Ag3-S5	2.353(2)
Cu1-S1	2.279(3)	Cu1-S2	2.243(2)
Cu1-S3	2.247(2)	Cu2-S4	2.254(2)
Cu2-S5	2.223(2)	Cu2-S6	2.250(2)
Ag1- Ag2	3.3100(11)	Ag1-Cu1	3.0161(13)
Ag1-Cu2	2.8936(13)	Ag1-S1	2.323(3)
Ag1-S4	2.342(2)	Ag2-Cu1	2.9644(13)
Ag2-Cu2	2.9980(13)	Ag2-S2	2.356(2)
Ag2-S6	2.352(2)	Ag3-Cu1	2.9015(13)
***A*-1**			
Atom-Atom	Bond length/ Å	Atom-Atom	Bond length/ Å
Ag1-Cu1	3.0100(14)	Ag3-Cu2	2.9841(13)
Ag3-S3	2.360(3)	Ag3-S5	2.348(3)
Cu1-S1	2.284(3)	Cu1-S2	2.243(3)
Cu1-S3	2.240(2)	Cu2-S4	2.253(3)
Cu2-S5	2.219(2)	Cu2-S6	2.246(2)
Ag1- Ag2	3.3048(11)	Ag1-Cu1	3.0100(14)
Ag1-Cu2	2.8899(14)	Ag1-S1	2.323(3)
Ag1-S4	2.338(3)	Ag2-Cu1	2.9606(13)
Ag2-Cu2	2.9922(13)	Ag2-S2	2.353(3)
Ag2-S6	2.346(2)	Ag3-Cu1	2.8947(14)

Table S3 Selected bond angles for *C*-**1** and *A*-**1.**

***C*-1**			
Atom-Atom-Atom	Bond angle/ °	Atom-Atom-Atom	Bond angle/ °
Cu1-Ag1-Ag2	55.65(3)	Cu2-Ag1-Ag2	57.33(3)
Cu2-Ag1-Cu1	96.46(4)	S1-Ag1-Ag2	87.94(6)
S1-Ag1-Cu1	48.42(6)	S1-Ag1-Cu2	142.70(7)
S1-Ag1-S4	167.53(9)	S4-Ag1-Ag2	102.93(6)
S4-Ag1-Cu1	143.53(7)	S4-Ag1-Cu2	49.64(6)
Cu1-Ag2-Ag1	57.14(3)	Cu1-Ag2-Cu2	95.35(3)
Cu2-Ag2-Ag1	54.34(3)	S2-Ag2-Ag1	101.35(6)
S2-Ag2-Cu1	48.22(6)	S2-Ag2-Cu2	141.55(6)
S6-Ag2-Ag1	86.74(6)	S6-Ag2-Cu1	141.22(6)
S6-Ag2-Cu2	47.90(6)	S6-Ag2-S2	170.37(8)
Cu1-Ag3-Cu2	96.84(4)	S3-Ag3-Cu1	49.22(6)
S3-Ag3-Cu2	142.03(7)	S5-Ag3-Cu1	141.13(6)
S5-Ag3-Cu2	47.33(6)	S5-Ag3-S3	169.62(8)
Ag2-Cu1-Ag1	67.20(3)	Ag3-Cu1-Ag1	70.56(3)
Ag3-Cu1-Ag2	74.05(3)	S1-Cu1-Ag1	49.69(7)
S1-Cu1-Ag2	97.73(7)	S1-Cu1-Ag3	116.35(8)
S1-Cu1- Ag1	113.74(7)	S2-Cu1-Ag2	51.55(7)
S2-Cu1-Ag3	109.31(8)	S2-Cu1-S3	130.08(10)
S2-Cu1-S1	112.73(9)	S3-Cu1-Ag1	103.07(7)
S3-Cu1-Ag2	124.92(8)	S3-Cu1-Ag3	52.86(7)
S3-Cu1-S1	116.72(9)	Ag1-Cu2-Ag2	68.34(3)
Ag1-Cu2-Ag3	71.03(3)	Ag2-Cu2-Ag2	72.29(3)
S4-Cu2-Ag1	52.35(7)	S4-Cu2-Ag2	115.60(7)
S4-Cu2-Ag3	105.67(7)	S5-Cu2-Ag1	118.91(7)
S5-Cu2-Ag2	105.61(7)	S5-Cu2-Ag3	51.10(6)
S5-Cu2-S4	122.36(9)	S5-Cu2-S6	123.63(9)
S6-Cu2-Ag1	99.57(7)	S6-Cu2-Ag2	50.84(6)
S6-Cu2-Ag3	120.21(7)	S6-Cu2-S4	113.57(9)
Cu1-S1-Ag1	81.88(9)	C1-S1-Ag1	107.2(4)
C1-S1-Cu1	105.2(4)	Cu1-S2-Ag2	80.23(8)

C7-S2-Ag2	107.1(3)	C7-S2-Cu1	111.7(3)
Cu1-S3-Ag3	77.92(8)	C13-S3-Ag3	105.7(3)
C13-S3-Cu1	103.8(3)	Cu2-S4-Ag1	78.01(8)
C19-S4-Ag1	107.6(3)	C19-S4-Cu2	113.2(3)
Cu2-S5-Ag3	81.57(8)	C25-S5-Ag3	106.3(3)
C25-S5-Cu2	110.1(3)	Cu2-S6-Ag2	81.26(8)
C31-S6-Ag2	105.9(3)	C31-S6-Cu2	105.8(3)

***A*-1**

Atom-Atom-Atom	Bond angle/ °	Atom-Atom-Atom	Bond angle/ °
Cu1-Ag1-Ag2	55.68(3)	Cu2-Ag1-Ag2	57.30(3)
Cu2-Ag1-Cu1	96.33(4)	S1-Ag1-Ag2	88.06(7)
S1-Ag1-Cu1	48.64(7)	S1-Ag1-Cu2	142.79(7)
S1-Ag1-S4	167.41(10)	S4-Ag1-Ag2	102.98(7)
S4-Ag1-Cu1	143.39(7)	S4-Ag1-Cu2	49.70(7)
Cu1-Ag2-Ag1	57.11(3)	Cu1-Ag2-Cu2	95.22(4)
Cu2-Ag2-Ag1	54.36(3)	S2-Ag2-Ag1	101.33(6)
S2-Ag2-Cu1	48.28(6)	S2-Ag2-Cu2	141.49(6)
S6-Ag2-Ag1	86.60(6)	S6-Ag2-Cu1	141.05(7)
S6-Ag2-Cu2	47.90(6)	S6-Ag2-S2	170.46(8)
Cu1-Ag3-Cu2	96.80(4)	S3-Ag3-Cu1	49.19(6)
S3-Ag3-Cu2	141.92(7)	S5-Ag3-Cu1	141.13(6)
S5-Ag3-Cu2	47.36(6)	S5-Ag3-S3	169.66(8)
Ag2-Cu1-Ag1	67.21(3)	Ag3-Cu1-Ag1	70.67(3)
Ag3-Cu1-Ag2	74.15(3)	S1-Cu1-Ag1	49.77(7)
S1-Cu1-Ag2	97.73(7)	S1-Cu1-Ag3	116.54(8)
S1-Cu1- Ag1	113.68(7)	S2-Cu1-Ag2	51.54(7)
S2-Cu1-Ag3	109.43(8)	S3-Cu1-S2	130.30(10)
S2-Cu1-S1	112.51(9)	S3-Cu1-Ag1	103.07(8)
S3-Cu1-Ag2	125.06(8)	S3-Cu1-Ag3	52.86(7)
S3-Cu1-S1	116.68(10)	Ag1-Cu2-Ag2	68.34(3)
Ag1-Cu2-Ag3	71.11(3)	Ag2-Cu1-Ag1	67.21(3)
S4-Cu2-Ag1	52.30(7)	S4-Cu2-Ag2	115.60(8)
S4-Cu2-Ag3	105.58(7)	S5-Cu2-Ag1	118.99(8)

S5-Cu2-Ag2	105.74(7)	S5-Cu2-Ag3	51.10(7)
S5-Cu2-S4	122.25(9)	S5-Cu2-S6	123.91(10)
S6-Cu2-Ag1	99.35(7)	S6-Cu2-Ag2	50.79(7)
S6-Cu2-Ag3	120.37(7)	S6-Cu2-S4	113.40(9)
Cu1-S1-Ag1	81.59(9)	C1-S1-Ag1	107.5(3)
C1-S1-Cu1	104.4(4)	Cu1-S2-Ag2	80.17(8)
C7-S2-Ag2	106.3(3)	C7-S2-Cu1	110.7(3)
Cu1-S3-Ag3	77.95(8)	C13-S3-Ag3	105.7(3)
C13-S3-Cu1	104.0(3)	Cu2-S4-Ag1	77.99(8)
C19-S4-Ag1	107.5(3)	C19-S4-Cu2	113.3(3)
Cu2-S5-Ag3	81.54(8)	C25-S5-Ag3	106.9(3)
C25-S5-Cu2	109.3(3)	Cu2-S6-Ag2	81.30(8)
C31-S6-Ag2	105.6(3)	C31-S6-Cu2	106.0(3)

Table S4 Crystallographic data and structure refinements results for **2-5**

Cluster complex	**2**	**3**	**4**	**5**
Empirical formula	$C_{57}H_{88}Ag_3Cl_4Cu_2PS_6$	$C_{57}H_{88}Ag_3Cl_2Cu_2PS_6$	$C_{58}H_{88}Ag_3Cl_2Cu_2PS_6$	$C_{48}H_{74}Ag_3Cu_2PS_6$
Formula weight	1589.09	1518.19	1530.20	1325.09
Temperature/K	190.00(10)	190.00(10)	190.01(10)	190.01(10)
Crystal system	triclinic	monoclinic	monoclinic	triclinic
Space group	$P\bar{1}$	$P2_1/n$	$P2_1/n$	$P\bar{1}$
a/Å	13.8063(4)	14.1108(5)	14.0658(5)	12.5420(7)
b/Å	14.8132(5)	23.2804(12)	23.5120(11)	12.5516(7)
c/Å	18.4926(6)	20.4826(10)	20.5437(9)	19.3067(10)
α/°	74.687(3)	90	90	103.801(4)
β/°	84.949(2)	96.203(4)	95.858(3)	93.205(4)
γ/°	72.840(3)	90	90	97.260(4)
Volume/Å^3	3485.2(2)	6689.2(5)	6758.6(5)	2916.2(3)
Z	2	4	4	2
ρ_{calc}g/cm^3	1.514	1.508	1.504	1.509
μ/mm 1	1.817	1.812	1.794	1.978
F(000)	1616.0	3096.0	3120.0	1344.0
Crystal size/mm^3	0.332×0.205× 0.117	0.481×0.177×0.148	0.4×0.3×0.2	0.37×0.226×0.168
Radiation	Mo Kα (λ = 0.71073)	Mo Kα (λ = 0.71073)	Mo Kα (λ = 0.71073)	Mo Kα (λ = 0.71073)
2θ range for data collection/°	3.82° to 58.984°	4° to 59.146°	3.996° to 59.172°	4.452° to 58.962°
Index ranges	-18≤ h ≤ 17, -19 ≤ k ≤ 19, -24 ≤ l ≤ 25	-19≤ h ≤ 18, -17 ≤ k ≤ 31, -27 ≤ l ≤ 28	-17≤ h ≤ 19, -28 ≤ k ≤ 32, -26 ≤ l ≤ 25	-15≤ h ≤ 16, -15 ≤ k ≤ 16, -26 ≤ l ≤ 26
Reflections collected	32492	38176	45165	27325
Independent reflections	16131 [R_{int} = 0.0351, R_{sigma} = 0.0676]	15726 [R_{int} = 0.0394, R_{sigma}= 0.0660]	15919 [R_{int} = 0.0456, R_{sigma} = 0.0683]	13552 [R_{int} = 0.0322, R_{sigma} = 0.0584]
Data/restraints/parameters	16131/90/656	15726/100/687	15919/33/650	13552/0/559
Goodness-of-fit on F^2	1.023	1.031	1.022	1.037
Final R indexes [I>=2σ(I)]	R_1=0.0569, wR_2=0.1298	R_1=0.0644, wR_2=0.1593	R_1=0.0625, wR_2=0.1505	R_1=0.0536, wR_2=0.1415
Final R indexes [all data]	R_1=0.0860, wR_2=0.1464	R_1=0.1028, wR_2=0.1813	R_1=0.1056, wR_2=0.1751	R_1=0.0753, wR_2=0.1553

Supplementary references

[S1] Z. Wang, H.-F. Su, Y.-Z. Tan, S. Schein, S.-C. Lin, W. Liu, S.-A. Wang, W.-G. Wang, C.-H. Tung, D. Sun and L.-S. Zheng, *Proc. Ntl. Acad. Sci. U. S. A*., **2017**, 114, 12132.

[S2] CrysAlisPro, Rigaku OD, The Woodlands, TX, 2015.

[S3] L. Palatinus and G. Chapuis, *J. Appl. Crystallogr*., **2007**, 40, 786.

[S4] G. M. Sheldrick, *Acta. Crystallogr., Sect. C*., **2015**, 71, 3.

[S5] O. V. Dolomanov, L. J. Bourhis, R. J. Gildea, J. A. K. Howard and H. Puschmann, *J. Appl. Crystallogr.,* **2009**, 42, 339.

[S6] A. L. Spek, *Acta. Crystallogr., Sect. D*., **2009**, *61*, 148.

[S7] F. Neese, *ORCA, version 4.2.0,* Software update: the ORCA program system, version 4.0, WIREs Comput Mol Sci, **2017**, 8, e1327.

[S8] a) A. D. Becke, *Phys. Rev. A* **1988**, 38, 3098-3100; b) J. P. Perdew, *Phys. Rev. B* **1986**, 33, 8822.

[S9] F. Weigend and R. Ahlrichs, *Phys. Chem. Chem. Phys*. **2005**, 7, 3297.

[S10] H. Shen, Z. Xu, L.-Z. Wang, Y.-Z. Han, X.-H. Liu, S. Malola, B. K. Teo, H. Häkkinen and N.-F. Zheng, *Angew. Chem. Int. Ed*., **2021**, 60, 22411.

[S11] S. Knoppe, I. Dolamic and T. Bürgi, *J. Am. Chem. Soc.,* **2012**, 134, 13114.